In situ plasma diagnostics study of a commercial high-power hollow cathode magnetron deposition tool

Liang Meng, Ramasamy Raju, Randolph Flauta,[a] Hyungjoo Shin, and David N. Ruzic[b]
Center for Plasma-Material Interactions, University of Illinois at Urbana-Champaign, Urbana, Illinois 61801

Douglas B. Hayden
Novellus Systems Inc, 4000 N. First Street, San Jose, California 95134

(Received 9 July 2009; accepted 9 November 2009; published 23 December 2009)

Using a newly designed and built plasma diagnostic system, the plasma parameters were investigated on a commercial 200 mm high-power hollow cathode magnetron (HCM) physical vapor deposition tool using Ta target under argon plasma. A three dimensional (3D) scanning radio frequency (rf)-compensated Langmuir probe was constructed to measure the spatial distribution of the electron temperature (T_e) and electron density (n_e) in the substrate region of the HCM tool at various input powers (2–15 kW) and pressures (10–70 mTorr). The T_e was in the range of 1–3 eV, scaling with decreasing power and decreasing pressure. Meanwhile, n_e was in the range of 4×10^{10}–1×10^{12} cm^{-3} scaling with increasing power and decreasing pressure. As metal deposits on the probe during the probe measurements, a self-cleaning plasma cup was designed and installed in the chamber to clean the tungsten probe tip. However, its effectiveness in recovering the measured plasma parameters was hindered by the metal layer deposited on the insulating probe tube which was accounted for the variation in the plasma measurements. Using a quartz crystal microbalance combined with electrostatic filters, the ionization fraction of the metal flux was measured at various input power of 2–16 kW and pressure of 5–40 mTorr. The metal ionization fraction reduced significantly with the increasing input power and decreasing gas pressure which were attributed to the corresponding variation in the ionization cross section and the residence time of the sputtered atoms in the plasma, respectively. Both the metal neutral and ion flux increased at higher power and lower pressure. The 3D measurements further showed that the ionization fraction decreased when moving up from the substrate to the cathode. © *2010 American Vacuum Society.*
[DOI: 10.1116/1.3271132]

I. INTRODUCTION

At shrinking critical dimensions (180 nm or less) with increasing aspect ratios (>5:1), ionized physical vapor deposition (I-PVD) began to overtake conventional PVD in integrated circuit (IC) manufacturing.[1–4] The use of I-PVD improves the bottom and sidewall coverage in the trench for Ta barrier and Cu seed layers due to the larger fraction of ionized metal species present in the plasma. By applying a bias to the substrate, the metal ions are accelerated normally into the trenches and vias. The particles that reach the substrate consist of directed ions and isotropic neutrals. Thus, control of the flux population in I-PVD systems is important especially when depositing at narrower trenches for the next generation ICs.[5] Despite the projections of having PVD be replaced for the next generation of interconnect technology, I-PVD-based processes may prove more viable especially for liner seed through 45 nm.[6]

The hollow cathode magnetron (HCM) is one type of high density plasma tools developed for I-PVD. Unlike other I-PVD approaches where postionization of sputtered or evaporated metal atoms are made using secondary inductively coupled or electron cyclotron resonance plasmas,[7–10] the HCM uses a single dc power supply to both sputter and ionize the target material. The downstream ionization is achievable with magnetic field confinement of the plasma within the three dimensional (3D) target geometry. The magnetic field confinement promotes oscillations of hot electrons inside the cathode to enhance the ionization, ion bombardment of inner walls, and other subsequent processes.[11] At the same power, the HCM exhibits plasma density one to two orders of magnitude higher than that of conventional planar magnetrons.[12]

To better understand the fundamental mechanisms of the HCM devices and consequently obtain the control necessary to ensure highly conformal and uniform barrier and seed layers, it is desirable to use a number of plasma diagnostics to study the detailed influences of parameter variation on the plasmas. Such diagnostics could also be necessary for the other commercial tools utilizing plasmas: PVD, etch, strip, high density plasma chemical vapor deposition, plasma enhanced chemical vapor deposition, etc. For HCM, however, due to intense deposition environment at these special plasma conditions with nonstandard geometry, plasma diagnostics are especially required to provide both flexible and reliable measurements. Langmuir probe is a traditional plasma diagnostics technique, despite of the intrinsic draw-

[a]Electronic mail: rflauta@illinois.edu
[b]Electronic mail: druzic@illinois.edu

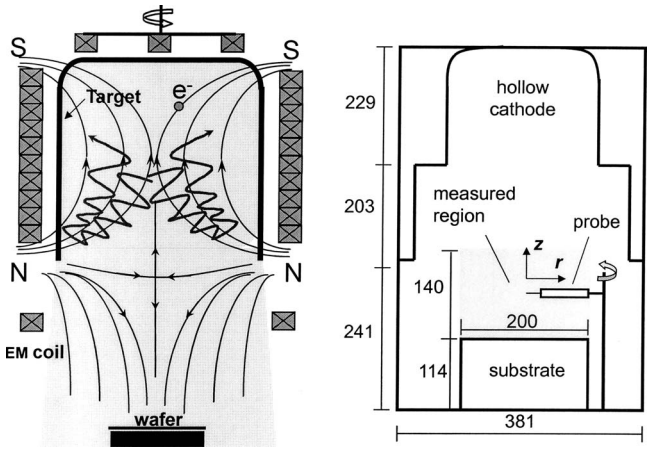

FIG. 1. Schematic of the HCM with dimension in millimeters. (Left) The magnetic field configuration acting as a "magnetic mirror." (Right) The location of Langmuir probe inside the chamber with a scanning area of 150 mm in the z direction and 100 mm from the center to the substrate edge in the r direction.

backs of plasma perturbation and surface contamination.[13] The nonintrusive probe has been explored a lot that the planar probe with guarded plane[14] and the dual floating Langmuir probe[15] are claimed to have minimum perturbations. However, they are usually limited to the application near the substrate or plasma boundary, not suitable for our 3D plasma diagnostics. The surface contamination on the probe has been investigated in the insulating material generating plasma,[16,17] but is seldom done in a strong metal plasma. In this article, a cylindrical Langmuir probe was first evaluated and then used to characterize the plasma parameters essential for understanding the HCM as a deposition tool. Like many I-PVD tools, the HCM was specifically developed to provide high metal ionization. Thus, a diagnostic tool to measure such ionization fraction is also desirable. In this study, an *in situ* method using a gridded energy analyzer (GEA) and a quartz crystal microbalance (QCM) was used to determine the ionization fraction.[5,18]

II. EXPERIMENT

The experiments were carried out in a 200 mm INOVA HCM commercial tool, 673 mm in height and 381 mm in inner diameter as shown in Fig. 1. The hollow cathode at the top consists of a tantalum (Ta) target in a shape of an inverted bucket. The 200 mm diameter substrate was set at 114 mm higher than the bottom surface of the chamber. Magnetic fields were adjusted to form a magnetic separatrix at the opening of the HCM to prevent electron loss and result in high density plasma confinement within the hollow cathode. Both a cryopump and a turbopump were used to evacuate the chamber to a base pressure of $\sim 10^{-7}$ Torr. The target was sputtered using argon (Ar) gas with pressures that ranged between 5 and 70 mTorr. The input power for the HCM source was up to 16 kW during operation with the target well protected with water cooling.

A cylindrical tungsten (W) Langmuir probe with a tip length of 6.4 mm and diameter of 0.254 mm was fabricated and mounted on a rotary-linear arm as illustrated in Fig. 1. By linearly moving and sweeping the probe, the plasma parameters were measured at different vertical positions z up to 150 mm from substrate and different radial position r up to 100 mm from the center (i.e., from center to the edge of the 200 mm substrate). The electron temperature T_e and electron density n_e were obtained by analyzing the Langmuir probe I-V traces according to the Laframboise method described by Ruzic.[19] The input power and the pressure were varied to study their influences on the spatial distributions of T_e and n_e. Before the probe measurements, several tests to study the reliability and reproducibility of the probe measurements were performed. An optimized procedure was developed for the probe measurements according to the study

Test 1. The probe was fixed in a certain position and kept collecting data for 30 min after the plasma was turned on (2 kW, 66 mTorr Ar). The obtained T_e and n_e varied with time. It should be noted that in this section of probe reliability test, T_e and n_e are actually the "apparent" values rather than real ones. Different factors were likely responsible for these variations. The accumulated metal deposition was first evaluated to sputter out the contamination on the tip using a secondary plasma cleaning cup as described in Sec. III A. Some other factors such as the initial plasma stability, temperature of HCM tool, and the temperature of the probe could also account for the variation in the apparent T_e and n_e. Further investigations were performed to study the effects of these factors and then try to avoid them during plasma measurements.

Test 2. The effects due to unstable plasma or temperature of HCM tool were studied. The plasma was turned on for 20 min during which the effects of plasma instability or temperature variation in the HCM tool on the plasma diagnostics were investigated. A special procedure was used to prevent the change in the probe temperature. The probe was only exposed to the plasma when collecting data which took about 30 s each time. After that, it was moved out of the plasma and shielded for 3 min to cool down and minimize the variation in the probe temperature. Also, the metal deposition on the probe was reduced. This shielding procedure was used for all the following experiments. This test revealed that waiting for 10 min after turning on the plasma is enough to stabilize the plasma and the tool temperature.

Test 3. In order to verify the influence of metal deposition on the probe surface, the probe was intentionally exposed to the plasma to get different degrees of metal deposition. The above procedures for probe shielding and plasma stabilization were used. After staying in the plasma for some time, the probe was moved out of the plasma and cooled down before being swept back to get a probe trace. The plasma measurements with different amounts of metal contamination were then compared.

Test 4. Finally, an experiment was designed to understand the respective influences of metal deposition on the probe tip and probe insulating body. The following three probes with different surface conditions were tested.

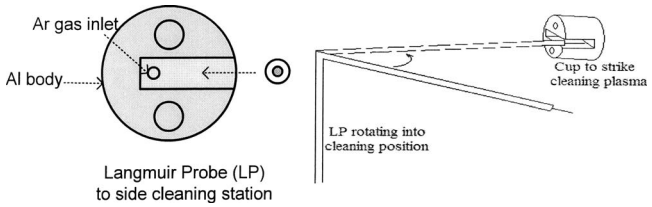

FIG. 2. Schematic diagram of Langmuir probe system with *in situ* plasma cup cleaning.

(1) New probe with both clean tip and clean alumina tube body.
(2) Probe with clean tube body but tip being deposited with metallic layer. This probe was prepared with the body covered with fiber tape before being deposited for 20 min. The glass tape was then removed to uncover the clean body.
(3) Probe with both the tip and body already deposited for 20 min in the plasma. The T_e and n_e were measured at an identical working condition: 2 kW of input power and 40 mTorr of pressure, and results were then compared with each other.

An *in situ* plasma cup was designed to remove the deposited thin film material on the probe surface utilizing a strong independent secondary plasma as shown in Fig. 2. The cup is an aluminum block of 76 mm in length and 51 mm in diameter. It has a side cleaning station of 51 mm in length and 12.7 mm in width so that the rf-compensated Langmuir probe can be moved inside the cup and cleaned. The cup was grounded while a negative bias of up to 2 kV could be applied to the probe tip sitting inside the cleaning station. An independent strong Ar plasma was generated to sputter off the deposited material layer from the probe tip.

To estimate the ionization fraction of the metal flux in the plasma, an electrostatic GEA was constructed and combined with a QCM. Figure 3 shows the schematic diagram of the GEA and the QCM where the GEA is located above the QCM. The GEA has a ceramic casing with an inner diameter of 30 mm. Three layers of stainless steel meshes are evenly placed inside with the gaps of 6.4 mm. The wire distance in the mesh is 0.282 mm with 50% transparency. The top mesh grid was grounded to minimize disturbance to the plasma while the middle grid (the electron repeller grid) was negatively biased at around −15 V to reduce the electron penetration. The bottom grid (the ion repeller grid) was applied with an adjustable voltage from −10 to 30 V.

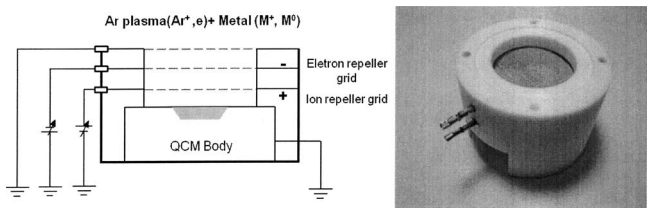

FIG. 3. (Left) Schematic of the GEA and QCM assembly; (Right) a real GEA with ceramic casing and ceramic disk to insulate the screens (top screen is not shown).

The total fluxes of metal ions and neutrals $\Phi_{\text{tot\_QCM}}$ admitted to the QCM sensor can be determined when the ion repeller grid was negatively biased. Then a positive bias was applied to the grid and gradually increased up to 30 V so that only the neutral flux $\Phi_{\text{N\_QCM}}$ reached the QCM. The ion flux $\Phi_{\text{ion\_QCM}}$ received by the QCM was obtained by subtracting the neutral flux from the total flux as given in Eq. (1). To calculate the actual ion flux $\Phi_{\text{ion\_plasma}}$ and neutral flux $\Phi_{\text{N\_plasma}}$ before entering the GEA, the transparency T_g due to three layers of grids was also taken into account as given in Eqs. (2) and (3). Moreover, as for the nondirectional neutral flux, the ceramic casing will shadow an extra fraction of neutrals from reaching the QCM sensor, which induces a geometrical factor G. A more specific description of the calculation of G was done by Green *et al.*[5] For the current GEA setup, $G=0.42$ was used in the calculation assuming an isotropic distribution of neutrals. For normally incident ions governed by electric field, the fluxes at the QCM sensor and that at the substrate are the same if there were no screens present and the factor G is simply unity as implied in Eq. (3). The $\Phi_{\text{ion\_plasma}}$ and $\Phi_{\text{N\_plasma}}$ were further used to determine the ionization fraction I.F. of the metal flux as given in Eq. (4),

$$\Phi_{\text{ion\_QCM}} = \Phi_{\text{tot\_QCM}} - \Phi_{\text{N\_QCM}}, \tag{1}$$

$$\Phi_{\text{N\_QCM}} = \Phi_{\text{N\_plasma}}(\text{G})(T_g)^3, \tag{2}$$

$$\Phi_{\text{ion\_QCM}} = \Phi_{\text{ion\_plasma}}(T_g)^3, \tag{3}$$

$$\text{I.F.} = \frac{\Phi_{\text{ion\_plasma}}}{\Phi_{\text{ion\_plasma}} + \Phi_{\text{N\_plasma}}} = \frac{\Phi_{\text{tot\_QCM}} - \Phi_{\text{N\_QCM}}}{\Phi_{\text{tot\_QCM}} - \Phi_{\text{N\_QCM}} + \Phi_{\text{N\_QCM}}/G}. \tag{4}$$

The individual effects of input power and pressure on the ionization efficiency were investigated. Since the GEA and QCM assembly was mounted on a rotary-linear manipulator, ionization fraction can also be measured at different locations.

III. RESULTS AND DISCUSSION

A. Metal deposition on the probe and its effects

For the probe test 1 described in Sec. II, the measured apparent T_e and n_e at different deposition times were compared in Fig. 4. Discrepancies were observed especially in the first 15 min after the plasma was turned on. This was likely due to the unstable plasma and gradual warming up of the chamber. Then the apparent T_e started to decrease slowly while n_e kept increasing. After 30 min, metal deposition on the insulating probe surface was obviously observed. In an attempt of minimizing the effect of the metal deposition on the probe, *in situ* cleaning of the probe tip was tried by negatively biasing the probe tip and initiating a secondary

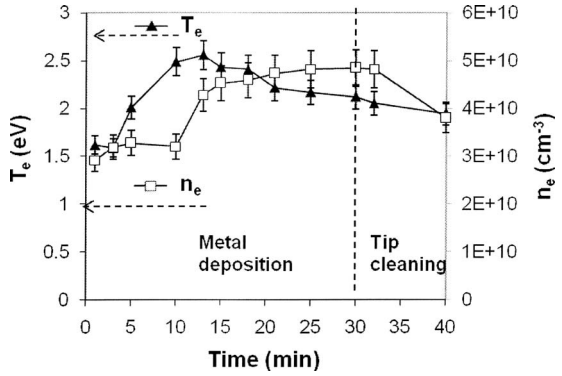

FIG. 4. Test 1 results: Apparent T_e and n_e measured with the probe staying in the plasma (2 kW, 66 mTorr) for 30 min. Then the probe was cleaned (for totally 10 min) and swept back again for measurements.

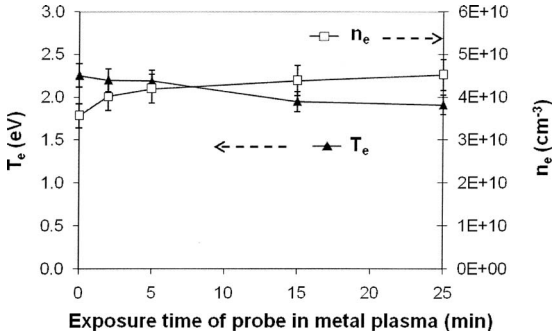

FIG. 6. Test 3 results: Apparent T_e and n_e measured at increasing total exposure time of probe in the plasma (2 kW, 40 mTorr). Plasma was stabilized and probe was shielded before exposure to plasma and measurement.

discharge with respect to the grounded plasma cup. Cleaning for 10 min reduced the obtained n_e which seemed to be of the right trend, but the apparent T_e continued to decrease and did not recover. The underlying mechanisms of the metal deposition effects were to be further explored before more effective cleaning can be achieved.

Test 2 was designed to confirm the effects of the unstable plasma and the change in HCM tool temperature based on the data in Fig. 4. By shielding the probe before measurements, variations in probe temperature and the metal deposition were greatly suppressed during the test. The measured plasma parameters at different times of plasma running are shown in Fig. 5. Within the first 10 min (especially the first 5 min), the apparent T_e and n_e varied for about 10% and 14%, respectively, after which the values became much more stable. The variations were only 2% and 3% as a comparison. Based on this test, the procedures of probe shielding and plasma stabilization were found quite effective to avoid inconsistent probe measurements and were adopted in the further probe diagnostics.

Test 3 measured the T_e and n_e after different exposure times to the metal plasma as shown in Fig. 6. The other factors such as the variation in the plasma itself, tool temperatures, and probe temperature were minimized during the process. After a total exposure time of 25 min in the plasma, the T_e was reduced by approximately 15% and n_e increased by 27%, which are attributed to the metal deposition on the probe. Referring to Fig. 4, it could be understood that the continuing variations in the apparent T_e and n_e after 15 min were caused by the same reason.

To further understand the mechanism of the effect of the probe surface condition on the plasma measurements, test 4 was designed using three probes with different surface conditions: (1) new probe, (2) probe with a clean tube body but deposited tip, and (3) probe with both the tip and the body deposited with metal for 20 min. n_e and T_e results showed that at the same plasma environment (2 kW, 40 mTorr), the values measured by the third probe were different with the other two probes as illustrated in Fig. 7(a). The variation in

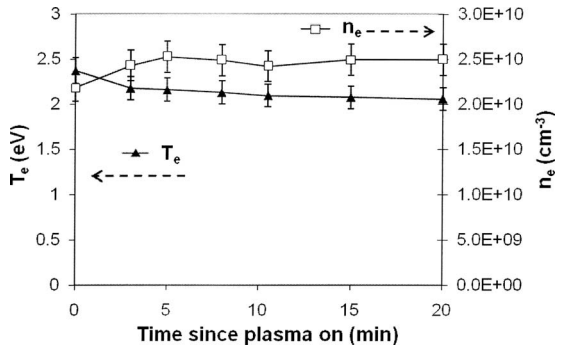

FIG. 5. Test 2 results: Apparent T_e and n_e measured using the procedure of shielding the probe before and after the measurements. Plasma condition: 1 kW, 40 mTorr.

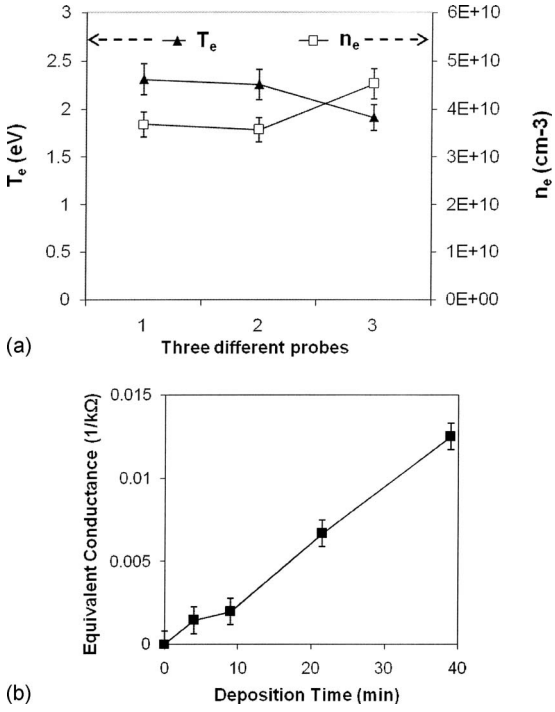

FIG. 7. (a) Test 4: Apparent T_e and n_e measured from different probes: (1) Clean probe, (2) probe with tip deposited, and (3) both tip and body deposited. (b) The equivalent conductivity (as the 1/resistance) measured between two fixed points on the probe body surface.

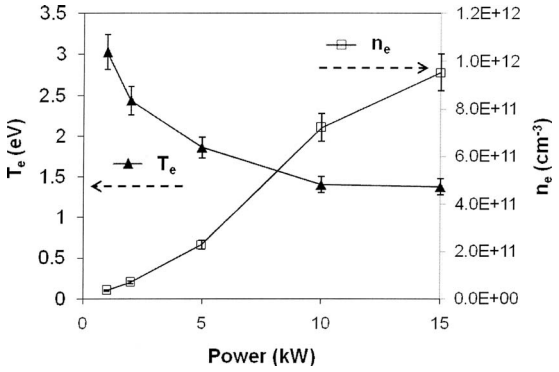

FIG. 8. T_e and n_e of Ar sputtering plasma at various input powers (66 mTorr, 102 mm above the substrate).

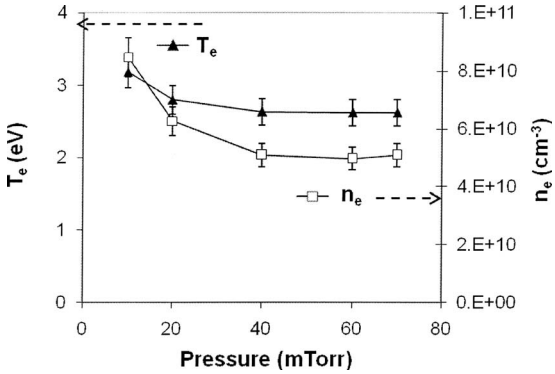

FIG. 9. T_e and n_e of Ar sputtering plasma at different pressures (2 kW, 102 mm above the substrate).

T_e and n_e can be attributed to the metal deposited on probe body rather than to that on the probe tip. The surface of probe body becomes increasingly conductive after exposure in the plasma for a certain period [Fig. 7(b)], so that the plasma around the conducting probe surface was possibly perturbed. It should be noted that the probe body was still well insulated from the tip. It could be concluded that not only the probe tip but also the whole probe body needs to be cleaned. An improved plasma cup is being constructed to negatively bias the probe body to meet this demand.

B. Probe diagnostics

Using the procedures developed in Sec. III A to improve the reproducibility of probe diagnostics, T_e and n_e were measured in the hollow cathode magnetron tool. Figure 8 shows the input power dependence of T_e and n_e at 102 mm above the substrate under a pressure of 66 mTorr. As the power increased from 1 to 15 kW, n_e increased from 3.6×10^{10} to 9.5×10^{11} cm^{-3} while T_e decreased from 3.0 to 1.4 eV. More intense plasma was generated at higher power implying a higher density of electrons. However, the electron energy was dramatically reduced due to more frequent inelastic collisions such as excitation and ionization of atoms.

Then plasma parameters were measured at various pressures (10–70 mTorr) with the probe located 102 mm above the substrate with the power held constant at 2 kW. A continuous decrease in n_e (from 8.5×10^{10} to 5.1×10^{10}) was observed when the pressure was increased from 10 to 70 mTorr, while T_e slightly decreased from 3.2 to 2.6 eV as shown in Fig. 9. The increased electron scattering at higher pressure reduces the electron energy. A substantial decrease in the ionization cross section led to a lower n_e despite the higher gas density.

The spatial distributions of T_e and n_e were measured and shown in Fig. 10. It indicated that T_e decreased as going further away from the source, which was caused by the energy loss while the electrons went through more collisions. In the radial direction, T_e was relatively uniform. As for n_e, it slightly decreased as it deviated from the center of the substrate and dropped more significantly near the substrate edge. The measurement at the higher position gave a higher n_e which was reasonable considering the diffusion of the plasma from the high density HCM source toward the substrate.

C. Ionization fraction measurement

The effect of input power on the ionization fraction was investigated with the GEA combined with the QCM. The QCM was fixed 25 mm higher from the center point of substrate. The metal deposition rates with and without ions were recorded at various powers and pressure conditions. The calibrated neutral and ion deposition rates on the substrate are

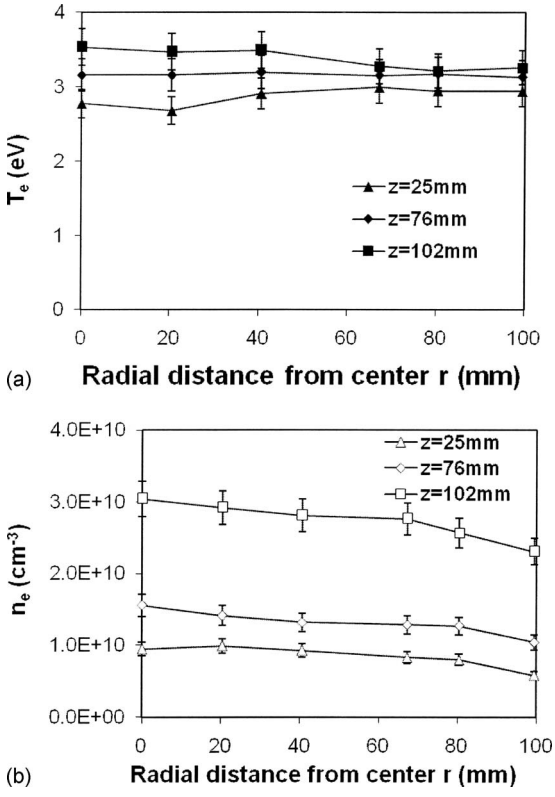

FIG. 10. Spatial distribution of (a) T_e and (b) n_e of a plasma as a function of radial distance r from the center and different heights z.

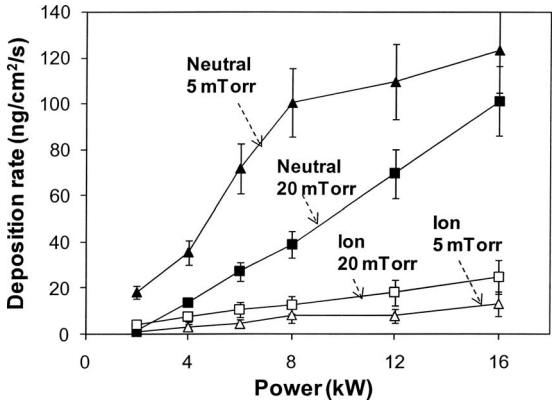

FIG. 11. Flux of metal neutrals and ions measured at 25 mm above the center of substrate, at various input powers and pressures.

shown in Fig. 11. It can be observed that both the neutral and ion flux increased with higher input power, which makes sense considering the increased sputtering rate and stronger plasma to ionize the sputtered atoms. Higher neutral deposition rate was also achieved at a lower pressure (5 mTorr), which was attributed to the higher sputtering yield due to higher discharge voltage and less particle loss to the chamber wall due to reduced scattering. Less scattering also implied that the directions of the neutrals are no longer isotropic but getting close to directional which is particularly suitable for the deposition of metallization layer at deep trenches (especially for target with a higher sputtering yield such as Cu). However, the QCM measurements indicated a reduction in ion flux at lower pressure resulting in lower ionization fraction. A more detailed investigation of effects of power and pressure on the ionization was given below.

Ionization fractions at varying power and pressure are illustrated in Fig. 12. The QCM was kept at the same position as before. It is obvious that low pressure leads to low ionization fraction. At 5 mTorr, the ionization fraction was always lower than 10%, whereas at 40 mTorr, the ionization fraction was in the range from 40% to nearly 100% depending on the power applied. The results are consistent with the results in Fig. 11.

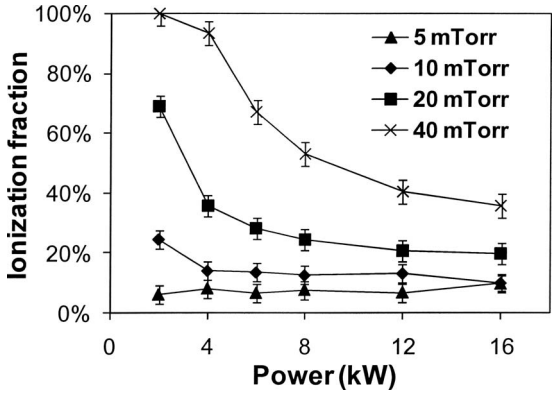

FIG. 12. Ionization fraction at varying power and working pressure, measured at 25 mm above the center of the substrate.

To understand the effects of pressure as well as power on the ionization fraction, the ionization process needs to be considered in the first place. In the HCM, the electrons are designed to be confined in the hollow cathode region by strong magnetic field, thus most of the ions are generated in the cathode region as the "source." These ions will then diffuse to the substrate. So it is important to know the reactions happening in the cathode. The ionization rate is proportional to the ionization cross section depending on the electron temperature T_e, electron density n_e, and the residence time of metal atoms in the hollow cathode. As the gas pressure is decreased, the residence time of atoms will be reduced due to less scattering, thus the chances of atoms being ionized will greatly decrease leading to a lower ionization fraction. For the T_e and n_e in the cathode, it is difficult to directly measure them, but they could be assumed to have the same trends versus pressure or power as those in the substrate region. According to Fig. 9, the effects of pressure on the T_e and n_e are not very significant, so the change in ionization cross section is a minor effect.

As shown in Fig. 12, an increase in power resulted in a decreasing trend of the ionization fraction. This seems to be somewhat *counterintuitive* since the plasma was more intense at higher power and the electron density n_e was shown to increase as previously shown in Fig. 8. But referring to Fig. 11, it is shown that the ion concentration actually increased almost linearly with the power, which makes sense. It is just because the concentration of neutral atoms increased more rapidly with power that the ionization fraction decreased. Considering again the reactions in the hollow cathode, the ionization cross section of atoms by electrons is sensitively dependent on the electron temperature T_e, which could be estimated as[20]

$$K_{iz} \approx K_{iz0} e^{-\varepsilon_{iz}/T_e}. \tag{5}$$

Here, K_{iz} is the ionization cross section, K_{iz0} is the preexponential factor, and ε_{iz} is the ionization energy. As the power increased from 2 to 16 kW (other conditions are not exactly the same), T_e in the substrate region decreased approximately from 3 to 1 eV (Fig. 8). Since these electrons were diffused from the source, the decreasing trend of T_e should also stand in the cathode region which greatly reduced the probability of ionization. Also, according to Juliano *et al.* the increased gas temperature at higher power will lead to a faster diffusion and thus shorter residence time.[21] As a result, the ionization fraction will be further reduced at higher power. A more accurate demonstration of the trends of ionization versus various pressure and power would require a detailed mathematical model of electron confinement, density profile, sputtering process of target, the ionization of the sputtered atoms in the cathode region, as well as the diffusion process to the substrate.

Since the QCM assembly was mounted to a rotary-linear arm, 3D measurements of the ionization fraction in the chamber were possible. At a discharge condition of 6 kW and 20 mTorr, the QCM was raised for to 152 mm from the center of the substrate toward the cathode. Here the change

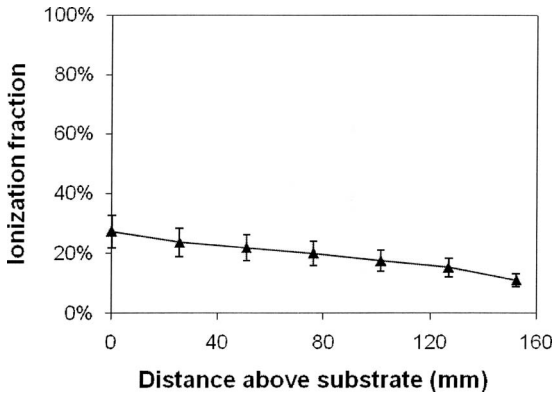

FIG. 13. Ionization fraction measured at different heights from the center of the substrate, at a power of 6 kW and a pressure of 20 mTorr.

in direction distribution of neutral atoms at different heights was neglected so that the same geometrical factor of 0.42 was used. Figure 13 shows that the ionization fraction was also observed to decrease when moving away from the substrate toward the source from 27% to 11%, respectively. The metal atoms arriving at the substrate travel for a longer average time in the bulk plasma than those collected at higher position which implies that an extra mount of atoms are ionized resulting in a higher ionization fraction. Also when moving from the source to the substrate, neutrals are continuously scattered out of the plasma to the chamber wall while ions have less loss due to the magnetic field confinement. This effect will also lead to the higher ionization fraction at lower position.

IV. CONCLUSION

Plasma diagnostics were used on a commercial 200 mm HCM deposition tool. A 3D scanning Langmuir probe was constructed and tested in Ar plasma using Ta target. Different factors affecting the reproducibility of the measurements were studied. Metal deposition on the probe due to the strong plasma environment was found to cause a considerable variation in the obtained electron temperature and electron density. Thus, an *in situ* plasma cup was designed to initiate a strong secondary plasma between the probe and the cup to sputter off the material deposited on the probe tip and the probe body. Cleaning of the probe tip with this plasma could only recover the measurements to a certain extent and a modification of the plasma cup is underway to further clean the whole probe body. To optimize the reliability of the probe diagnostics, special procedures were developed to avoid the variations in tool temperature and the probe temperature and minimize the metal deposition on the probe. In the HCM tool, as the power was increased from 2 to 15 kW, T_e values decreased from 3.0 to 1.4 eV while n_e increased from 3.6 $\times 10^{10}$ to 9.5×10^{11} cm^{-3}. The enhancement of plasma density in accordance to the power was found important for industrial-scale applications. The increase in n_e was achieved by lowering the pressure. The spatial distribution shows that at the substrate center n_e is higher than at edge while both T_e and n_e increased at a higher z position. The different number of collisions may account for these trends. The ionization fraction of the metal flux was estimated employing a QCM combined with electrostatic filters. It was found that at lower input power the ionization fraction increased due to the higher electron energy thus higher ionization cross section, while a higher pressure also increased the ionization fraction in virtue of a greater residence time of atoms in the plasma. The ionization fraction was also observed to increase when moving from source to the substrate.

[1] S. M. Rossnagel, Semicond. Int. **21**, 99 (1996).
[2] I. Hashim, V. Pavate, D. Peijun, B. Chin, D. Brown, and T. Nogami, Proc. SPIE **3508**, 58 (1998).
[3] B. Narayanan, C. Y. Li, L. Kangsoo, Y. Bo, W. J. Jie, P. D. Foo, and J. Xie, Proc. SPIE **3883**, 42 (1999).
[4] S. C. Chang, Y. L. Wang, and T. C. Wang, IEEE Trans. Semicond. Manuf. **17**, 384 (2004).
[5] K. M. Green, D. B. Hayden, D. R. Juliano, and D. N. Ruzic, Rev. Sci. Instrum. **68**, 4555 (1997).
[6] S. M. Rossnagel, R. Wisnieff, D. Edelstein, and T. S. Kuan, Tech. Dig. - Int. Electron Devices Meet. **2005**, 89.
[7] M. Yamashita, J. Vac. Sci. Technol. A **7**, 151 (1989).
[8] S. M. Rossnagel and J. Hopwood, J. Vac. Sci. Technol. B **12**, 449 (1994).
[9] T. Ono, C. Takahashi, and S. Matsuo, Jpn. J. Appl. Phys., Part 2 **23**, L534 (1984).
[10] C. Doughty, S. M. Gorbatkin, T. Y. Tsui, G. M. Pharr, and D. L. Medlin, J. Vac. Sci. Technol. A **15**, 2623 (1997).
[11] V. Vyas and M. J. Kushner, J. Vac. Sci. Technol. A **24**, 1955 (2006).
[12] K. F. Lai and Q. Lu, 26th IEEE International Conference on Plasma Sciences, California, 1999 (unpublished), p. 99.
[13] B. E. Cherrington, Plasma Chem. Plasma Process. **2**, 113 (1982).
[14] N. St. J. Braithwaite, J. P. Booth, and G. Cunge, Plasma Sources Sci. Technol. **5**, 677 (1996).
[15] L. J. Mahoney, C. W. Almgren, G. A. Roche, W. W. Saylor, W. D. Sproul, and H. V. Walde, U.S. Patent No. 6902646 (7 June 2005).
[16] G. Wehner and G. Medicus, J. Appl. Phys. **23**, 1035 (1952).
[17] R. J. D'Arcy, J. Phys. D: Appl. Phys. **7**, 1391 (1974).
[18] D. B. Hayden, D. R. Juliano, K. M. Green, D. N. Ruzic, C. A. Weiss, K. A. Ashtiani, and T. J. Licata, J. Vac. Sci. Technol. A **16**, 624 (1998).
[19] D. N. Ruzic, *Electrical Probes for Low Temperature Plasmas*, AVS Monograph Series (AVS Press, New York, 1994).
[20] M. A. Lieberman and A. J. Lichtenberg, *Principles of Plasma Discharge and Materials Processing* (Wiley, New York, 1994).
[21] D. R. Juliano, D. N. Ruzic, M. M. C. Allain, and D. B. Hayden, J. Appl. Phys. **91**, 605 (2002).